Pergamon

Int. J. Heat Mass Transfer. Vol. 39, No. 1, pp. 193–201, 1996

0017-9310/96 $9.50+0.00

0017-9310(95)00123-9

The influence of inner-wall motion on the linear stability of natural convection in a tall vertical annulus

J.-C. CHEN, G.-H. CHOU and C.-K. HSIEH

Department of Mechanical Engineering, National Central University, Chung-Li, Taiwan 32054, Republic of China

(*Received* 20 *November* 1994)

Abstract—The linear stability of natural convection in a tall vertical annulus with inner-cylinder motion was studied. The results show that the stability characteristics are significantly modified by the inner-cylinder motion. For a small Prandtl number fluid with a smaller radius ratio, the shear instability is dominant and the non-axisymmetric disturbance ($m = 1$) is most unstable no matter in which direction the inner cylinder is moving. For higher downward motion, the non-axisymmetric mode ($m = 2$) may replace modes $m = 0$ and 1 for some radius ratios. For higher Prandtl number fluids, the most unstable mechanism switches from a buoyant mode generated by the boundary layer near the outer cylinder to a buoyant mode induced by the boundary layer near the inner cylinder with an increase of curvature as the inner cylinder is moving.

1. INTRODUCTION

It is well known that a fluid in a tall vertical annulus rises near the hot surface and sinks near the cold surface due to the influence of a buoyancy force. When the temperature difference is small enough, the flow is parallel and the heat transfer across the gap is due to conduction only. When the temperature difference is higher than a certain value, the parallel flow becomes unstable to a complex flow pattern, and heat is transported by convection. The linear stability of natural convection in a tall vertical annulus with different wall temperatures has been studied by Choi and Korpela [1] and McFadden *et al.* [2]. Choi and Korpela considered only axisymmetric disturbances and found that the parallel flow is stabilized by the curvature and that for all Prandtl numbers the unstable parallel flows will become oscillatory traveling waves. The instability of a fluid with a small Prandtl number is due to the action of the shear force, while for a fluid with a high Prandtl number it is generated by the buoyant mode. McFadden *et al.* went a step further, considering both axisymmetric and non-axisymmetric disturbances. For $Pr = 0.71$ and 3.5, the least unstable disturbance is non-axisymmetric for smaller radius ratios and is axisymmetric for higher radius ratios. The results of McFadden *et al.* for $Pr = 0.71$ are consistent with those of Choi and Korpela in that the instability is set in by the shear mode. For $Pr = 3.5$, the non-axisymmetric shear mode is replaced by the axisymmetric buoyant one for some aspect ratios.

In recent years, the influence of a shear force on the stability properties of natural convection has become a subject of intense study. Mohamad and Viskanta [3] considered the linear stability of combined buoyancy and upper lid-driven shear flow in a shallow cavity. Their results showed that the upper lid motion stabilizes the flow for the Prandtl numbers they investigated. Chen and Hsieh [4] studied the influence of a shear force induced by the motion of the side wall on the linear stability of natural convection in a tall vertical slot. Three types of instability occurred: for smaller Prandtl number fluids, the instability is dominated by the shear mode; for higher Prandtl number fluids, a buoyant instability induced by the boundary layer near the fixed (unmoving) sidewall dominates; the buoyant instability induced by the boundary layer near the moving wall, which is subjected to a slight downward motion, occurs for Prandtl numbers close to 10.

In the present study, we consider the linear stability of natural convection in a tall vertical annulus with a heated inner cylinder under the influence of a shear force generated by the inner-cylinder motion. Both axisymmetric and non-axisymmetric disturbances are considered. The influence of the Reynolds and Prandtl numbers and radius ratio on the critical Grashof number, critical wave number and critical wave speed are all investigated.

2. FORMULATION AND SOLUTION

Consider two infinitely long, vertical concentric cylinders of annular gap L (outer radius minus inner radius, $R_2 - R_1$), enclosing a Newtonian fluid. The temperature of the inner cylinder, T_1, is higher than that of the outer one, T_2. The inner cylinder is moving up at a constant velocity U_p. Figure 1 shows a schematic of the annular geometry. A cylindrical coor-

NOMENCLATURE

c_r	non-dimensional critical wave speed
g	acceleration of gravity
Gr_c	critical Grashof number
k	axial wave number
L	gap of the annulus
m	azimuthal wave number
p	pressure
Pr	Prandtl number
Re	Reynolds number
t	time
T	temperature
ΔT	temperature difference
u, v, w	r, θ, z velocity components
U_p	moving velocity of the inner cylinder
U_b	characteristic velocity induced by buoyant force.

Greek symbols

α	thermal diffusivity
β	thermal expansion coefficient
η	radius ratio of the inner to outer cylinder
ν	kinematic viscosity
ρ	density
σ	complex growth rate.

Subscripts

c	critical value
1	inner cylinder
2	outer cylinder.

Superscripts

$\bar{}$	base flow quantity
$'$	perturbation quantity.

dinate system is chosen with the positive z axis in the direction opposite to the gravity g. The temperature difference is assumed sufficiently small so that the density is treated as a constant everywhere in the governing equation, except in the gravitational term. This is the so-called Boussinesq approximation. Accordingly, the kinematic viscosity ν, thermal diffusivity α and thermal expansion coefficient β are assumed to be constant.

The governing equations are taken to be the Navier–Stokes equations in cylindrical coordinates (r, θ, z) for the velocity components (u, v, w), pressure p, and temperature T. The equations are made dimensionless by scaling length by the annular gap L, temperature by the temperature difference ΔT between the cylinders, time by L^2/ν, fluid velocity by $U_b = g\beta L^2 \Delta T/\nu$ and pressure by ρU_b^2, where ρ is the density. The governing equations can be cast in the following non-dimensional forms with the same notations for convenience:

$$\frac{\partial u}{\partial r} + \frac{u}{r} + \frac{1}{r}\frac{\partial v}{\partial \theta} + \frac{\partial w}{\partial z} = 0 \tag{1a}$$

$$\frac{\partial u}{\partial t} + Gr\left(u\frac{\partial u}{\partial r} + \frac{v}{r}\frac{\partial u}{\partial \theta} + w\frac{\partial u}{\partial z} - \frac{v^2}{r}\right) = -Gr\frac{\partial p}{\partial r} + \left(\nabla^2 - \frac{1}{r^2}\right)u - \frac{2}{r^2}\frac{\partial v}{\partial \theta} \tag{1b}$$

$$\frac{\partial v}{\partial t} + Gr\left(u\frac{\partial v}{\partial r} + \frac{v}{r}\frac{\partial v}{\partial \theta} + w\frac{\partial v}{\partial z} + \frac{uv}{r}\right) = -\frac{Gr}{r}\frac{\partial p}{\partial \theta} + \left(\nabla^2 - \frac{1}{r^2}\right)v + \frac{2}{r^2}\frac{\partial u}{\partial \theta} \tag{1c}$$

$$\frac{\partial w}{\partial t} + Gr\left(u\frac{\partial w}{\partial r} + \frac{v}{r}\frac{\partial w}{\partial \theta} + w\frac{\partial w}{\partial z}\right) = -Gr\frac{\partial p}{\partial z} + \nabla^2 w + T^* \tag{1d}$$

$$\frac{\partial T^*}{\partial t} + Gr\left(u\frac{\partial T^*}{\partial r} + \frac{v}{r}\frac{\partial T^*}{\partial \theta} + w\frac{\partial T^*}{\partial z}\right) = \frac{1}{Pr}\nabla^2 T^* \tag{1e}$$

where $Gr = g\beta L^3 \Delta T/\nu^2$ is the Grashof number and $T^* = (T - T_0)$ the non-dimensional temperature difference measured relative to a reference state in equilibrium.

A steady, vertical parallel flow is assumed for the annulus with the form $(u, v, w, T, p) = [0, 0, w(r), T(r),$

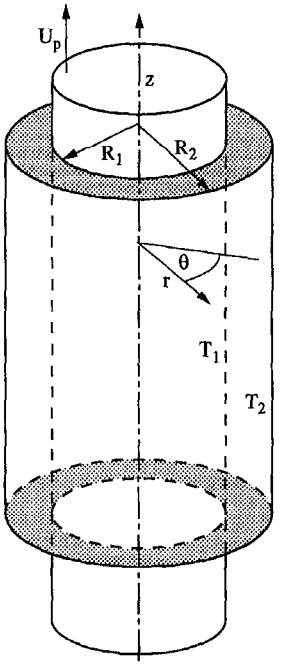

Fig. 1. Schematic of the annular geometry.

$p(z)$]. Under this assumption equation (1a)–(1d) can be reduced to

$$-Gr\frac{dp}{dz}+\frac{1}{r}\frac{d}{dr}\left(r\frac{dw}{dr}\right)+(T-T_0)=0 \quad (2a)$$

$$\frac{d}{dr}\left(r\frac{dT}{dr}\right)=0 \quad (2b)$$

with boundary conditions

$$w\left(\frac{\eta}{1-\eta}\right)=\frac{Re}{Gr} \quad (2c)$$

$$w\left(\frac{1}{1-\eta}\right)=0 \quad (2d)$$

$$T\left(\frac{\eta}{1-\eta}\right)=1 \quad (2e)$$

$$T\left(\frac{1}{1-\eta}\right)=0 \quad (2f)$$

where $\eta = R_1/R_2$ is the radius ratio and $Re = U_pL/\nu$ the Reynolds number.

The non-dimensional base temperature profile can be readily obtained from equations (2b), (2e) and (2f) as

$$T=\frac{1}{\ln\eta}\ln[(1-\eta)r]. \quad (3)$$

Note that the pressure gradient explicitly involved in equation (2a) is induced by the flow related to the inner moving cylinder; because of its linearity, the problem can be considered as the superposition of the forced (isothermal) flow, w_1, and the buoyancy-driven flow, w_2. The solutions of w_1 and w_2, after integrating twice and using the boundary conditions, are given by

$$w_1(r)=Ar^2+B\ln r+C \quad (4a)$$

$$w_2(r)=-\frac{r^2}{4\ln\eta}\ln[(1-\eta)r]+\frac{r^2}{4\ln\eta}+\frac{T_0r^2}{4}+D\ln r+E \quad (4b)$$

where the values of A, B, C, D, E and T_0 are given in the Appendix. Thus, the superposition of equation (4a) and (4b) gives the combined (forced and buoyancy-driven) flow.

The infinitesimal disturbances were put into the governing equations using the following transformations:

$$(u,v,w,p,T^*)=(0,0,\bar{w},\bar{p},\bar{T}^*)+(u',v',w',p',T'). \quad (5)$$

After substituting into the governing equations and boundary conditions, the portion resulting solely from the basic state was eliminated, the second- and higher-order terms were ignored, and normal modes of the form below with periodic disturbances in both the θ- and z-directions were assumed.

$$f'=f(r)\exp(ikz+im\theta-i\sigma t) \quad (6)$$

where $f(r)$ is the complex amplitude function, and k and m are disturbance wave numbers in the axial and azimuthal directions, respectively. The complex eigenvalue σ

$$\sigma=\sigma_r+i\sigma_i \quad (7)$$

contains the growth rate σ_i and the frequency σ_r. The imaginary part of σ (i.e. σ_i) determines the stability ($\sigma_i<0$) or instability ($\sigma_i>0$) of the basic flow. The condition $\sigma_i=0$ corresponds to marginal stability.

The linear disturbance equations become

$$Du+\frac{u}{r}+\frac{im}{r}v+ikw=0 \quad (8a)$$

$$D^2u+\frac{Du}{r}-Gr\,Dp-\left(\frac{m^2}{r^2}+k^2+\frac{1}{r^2}\right)u-\frac{2im}{r^2}v=ikGr\bar{w}u-i\sigma u \quad (8b)$$

$$D^2v+\frac{Dv}{r}-\frac{imGr}{r}p-\left(\frac{m^2}{r^2}+k^2+\frac{1}{r^2}\right)v+\frac{2im}{r^2}u=ikGr\bar{w}v-i\sigma v \quad (8c)$$

$$D^2w+\frac{Dw}{r}-ikGrp-\left(\frac{m^2}{r^2}+k^2\right)w+T=Gr\left(\frac{d\bar{w}}{dr}\right)u+ikGr\bar{w}-i\sigma w \quad (8d)$$

$$\frac{1}{Pr}\left(\frac{DT}{r}+D^2T-\frac{m^2}{r^2}T-k^2T\right)=Gr\left(\frac{d\bar{T}}{dr}\right)u+ikGr\bar{w}T-i\sigma T \quad (8e)$$

where $D=\partial/\partial r$ denotes partial differentiation with respect to r. The boundary conditions remains as;

$$u=v=w=T=0 \quad \text{at} \quad r=\eta/(1-\eta) \quad \text{and} \quad r=1/(1-\eta). \quad (9)$$

The disturbance equations (8) with boundary conditions (9) are solved numerically by using a standard shooting procedure without orthonormalization. In this numerical procedure, a fourth-order Runge–Kutta scheme is used to integrate the disturbance equations from $r=\eta/(1-\eta)$ or $r=1/(1-\eta)$. The number of integration steps employed in the calculations is 400. From these conditions and subsequent uses of Newton's method, values of Gr and σ corresponding to marginal stability are obtained for fixed k, Re, Pr, m and η. For the given values of Re and Pr, the critical Grashof number Gr_c is the smallest marginal value of Gr over the space of wave number k.

3. RESULTS AND DISCUSSION

The calculations were performed for $Pr = 0$, 0.1, 0.71 and 20 with $Re = 0$, 50, -50, -100 and -150. The critical values for various radius ratios are presented in Figs. 2–5. As $\eta \to 1$, the stability boundaries of the flow in a vertical annulus are nearly consistent with those in a vertical slot predicted by Chen and Hsieh [4].

Figure 2 shows the plots of the critical Grashof number Gr_c vs the radius ratio η for different values of Re with $Pr = 0.71$. The instability is found to be dominated by the shear mode. For $Re = 0$, 50, -50 and -100, the critical values of Gr_c for an axisymmetric disturbance ($m = 0$) are slightly less than those for a non-axiymmetric disturbance ($m = 1$) for higher radius ratios. For smaller radius ratios, the non-axisymmetric disturbance ($m = 1$) becomes less unstable. The radius ratio which marks the transition between $m = 0$ and $m = 1$ is about $\eta = 0.43$, which is very close to that predicted by of McFadden *et al.* [2], and may change insignificantly with the variation of the Reynolds number. For $Re = -150$, the most unstable disturbance is still axisymmetric for $\eta > 0.58$. The most unstable mode is $m = 2$ for $0.23 < \eta < 0.58$, while it becomes $m = 1$ for $\eta < 0.23$. The present results also show that the flow is stabilized by the downward motion of the inner cylinder. It is initially destabilized by smaller upward motion, and then stabilized by faster upward motion even though this is not shown in Fig. 2. The results are consistent with those predicted by Chen and Hsieh [4].

Figure 3 shows the variation of the critical Grashof number with the radius ratio for different Prandtl and Reynolds numbers. As mentioned by Hart [5] and Choi and Korpela [1], the instability of small Prandtl number fluids is induced by the shear mode while that of high Prandtl number fluids is generated by the buoyant mode. When the shear mode is dominant ($Pr = 0$, 0.1 and 0.71), the results show that Gr_c for $Re = 0$, 50, -50 and -100 increases as η decreases. This is due to the destabilizing effect of curvature. The results of $Re = 0$ [Fig. 3(a)] are consistent with the predictions of Choi and Korpela [1] except $\eta < 0.43$ for $Pr = 0$, 0.1 and 0.71 where the non-axisymmetric mode ($m = 1$) is dominant. For $Re = -150$, the most unstable mode is $m = 1$ for smaller radius ratios. As the radius ratio increases, the non-axisymmetric mode $m = 1$ is replaced by $m = 2$. With a further increase of the radius ratio the axisymmetric mode ($m = 0$) becomes most unstable. The critical Grashof number increases with the radius ratio when the mode $m = 1$ is dominant. When the mode $m = 2$ is most unstable, the critical Grashof number decreases initially and then increases as the radius ratio increases. When the instability is induced by $m = 0$, the critical Grashof number decreases as the radius ratio increases.

For $Pr = 20$, the instability is generated by the buoyant mode and the axisymmetric disturbance is most unstable. Choi and Korpela [1] and Chen and Hsieh [4] showed that for a vertical slot without sidewall motion, the buoyant instability causes two oscillatory traveling waves moving in opposite directions. Choi and Korpela also showed that with the introduction of curvature only a single traveling wave in the direction opposite to gravity exists when buoyant instability occurs. Chen and Hsieh showed that with sidewall motion the buoyant instability for $Pr = 20$ is induced by the boundary layer near the fixed (unmoving) sidewall with a downward traveling velocity. Based on the results of Chen and Hsieh, we believe that the buoyant instability is generated by the boundary layer near the inner cylinder. In Fig. 3(a), the critical Grashof number for $Pr = 20$ decreases as the radius ratio decreases, when $Re = 0$. It is obvious that for $Pr = 20$ the flow is destabilized by the influence of curvature. The critical Grashof number for $Pr = 20$ is less than those for $Pr = 0$, 0.1 and 0.71. When $Re \neq 0$, the critical Grashof number initially increases with the radius ratio for smaller radius ratios, where the instability is caused by the boundary layer near the inner cylinder. After the critical Grashof number reaches a maximum value, it begins to decrease with an increasing radius ratio. For larger radius ratios, the instability is due to the boundary layer near the fixed outer cylinder. The maximum Grashof number occurs at the radius ratio where the transition between two buoyant modes appears. When $Re = 50$ [Fig. 3(b)], the critical Grashof number for $Pr = 20$ at the transition point ($\eta = 0.74$) is higher than those for smaller Prandtl number. The results for $Re = -150$ are not shown in Fig. 3(e) since the solutions do not converge very well. By comparison, the results show that for $Pr = 20$, the flow is stabilized by either upward or downward motion of the inner cylinder.

Figure 4 shows the plots of the critical wave number in the axial direction vs the radius ratio for different values of Re. The discontinuous points for the results of $Pr = 0$, 0.1 and 0.71 represent the locations where the transition between the different azimuthal wave numbers occurs. The critical wave number k_c for $Pr = 0$, 0.1 and 0.71 increases with the radius ratio η except at the transition point between $m = 1$ and $m = 2$ for $Re = -150$. For smaller Prandtl numbers, the critical number k_c for $Re < 0$ increases when Re decreases. From Figure 4, we conjecture that the critical wave number k_c decreases when Re increases. The present results are consistent with the results of the vertical slot [4]. As $Pr = 20$ and $Re \neq 0$, the critical wave number decreases with an increasing radius ratio for smaller radius ratios where the buoyant instability generated by the boundary near the inner cylinder is dominant. For larger radius ratio, the buoyant instability induced by the boundary layer near the outer cylinder becomes dominant and the critical wave number increases with an increase of the radius ratio.

Figure 5 demonstrates the variation of the critical wave speed, which is defined as $c_r = \sigma_r/(k_c\, Gr_c)$, with η for different Re and Pr. The critical wave speed for $Pr = 0$, 0.1 and 0.71 increases as the radius ratio

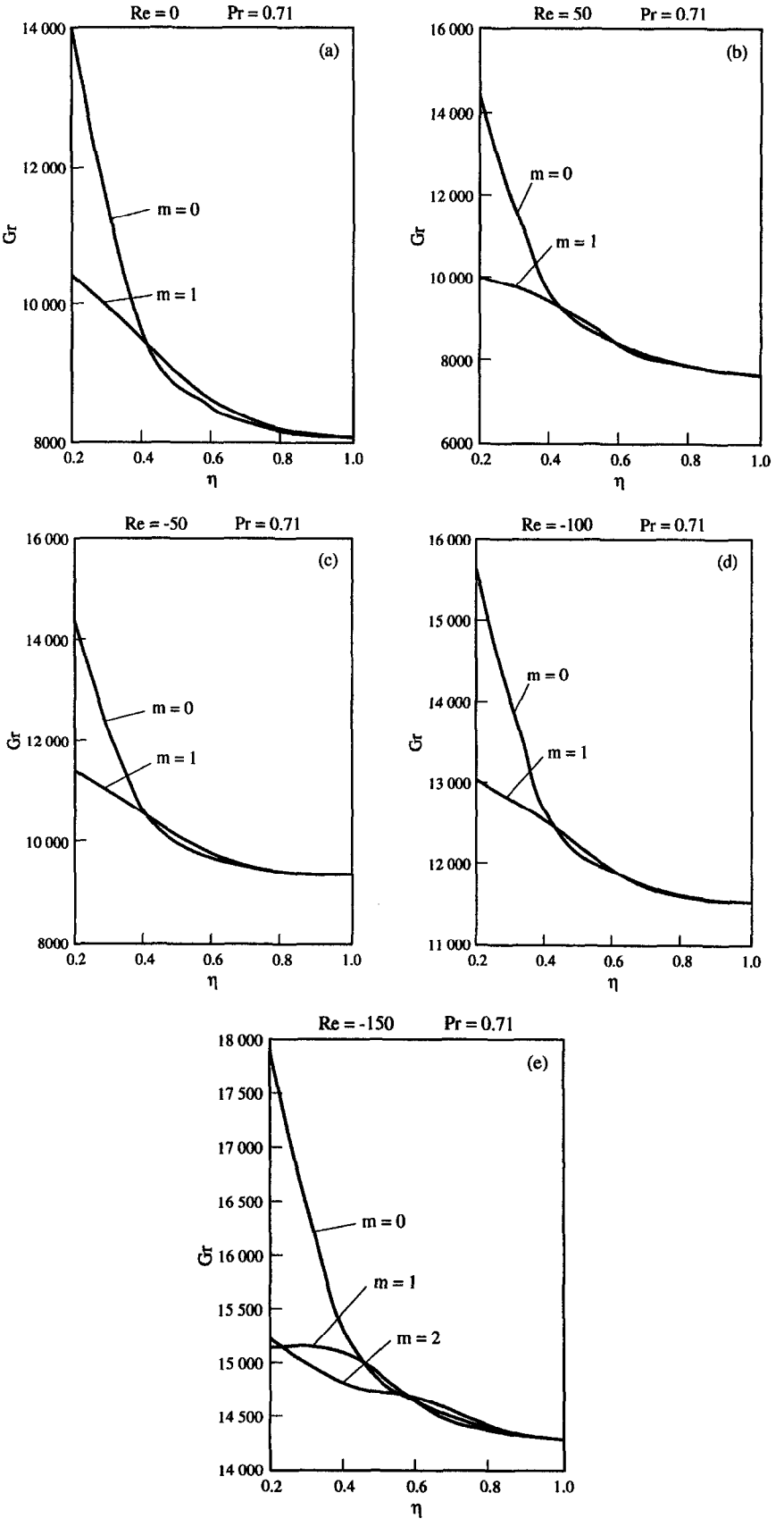

Fig. 2. The critical Grashof number for axisymmetric and non-axisymmetric disturbance as functions of the radius ratio: (a) $Re = 0$; (b) $Re = 50$; (c) $Re = -50$; (d) $Re = -100$; (e) $Re = -150$.

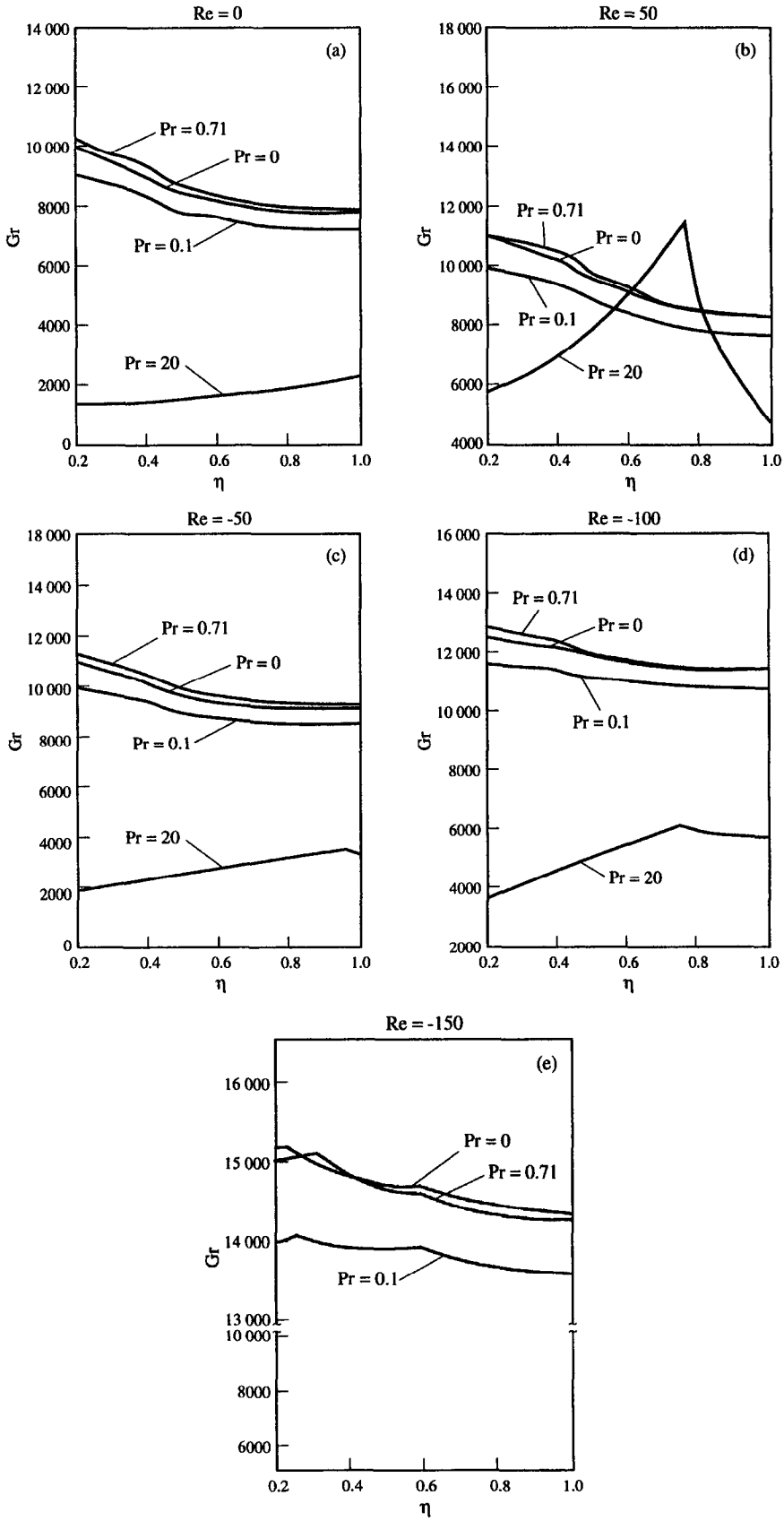

Fig. 3. The critical Grashof number for various values of the Prandtl number as functions of the radius ratio: (a) $Re = 0$; (b) $Re = 50$; (c) $Re = -50$; (d) $Re = -100$; (e) $Re = -150$.

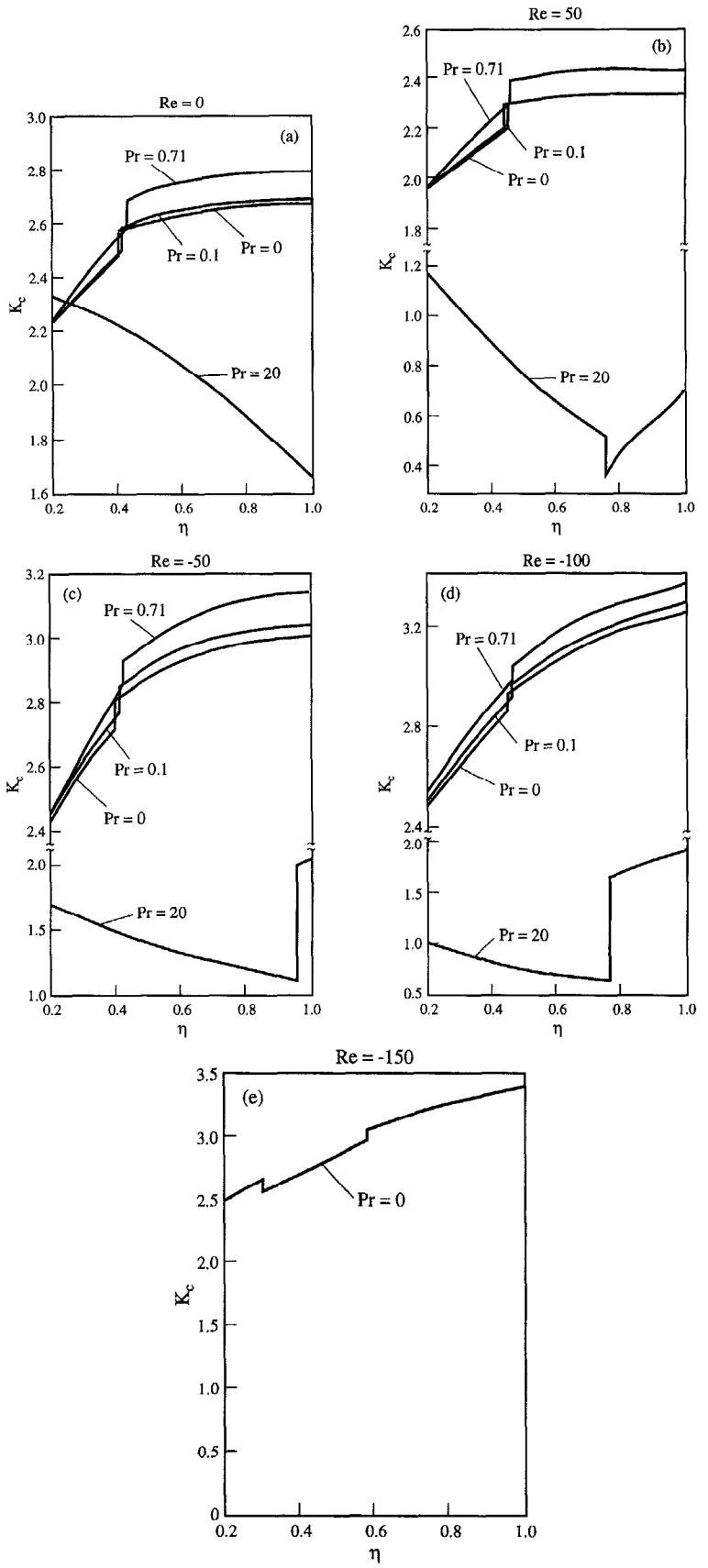

Fig. 4. The critical wave numbers for various values of the Prandtl number as functions of the radius ratio: (a) $Re = 0$; (b) $Re = 50$; (c) $Re = -50$; (d) $Re = -100$; (e) $Re = -150$.

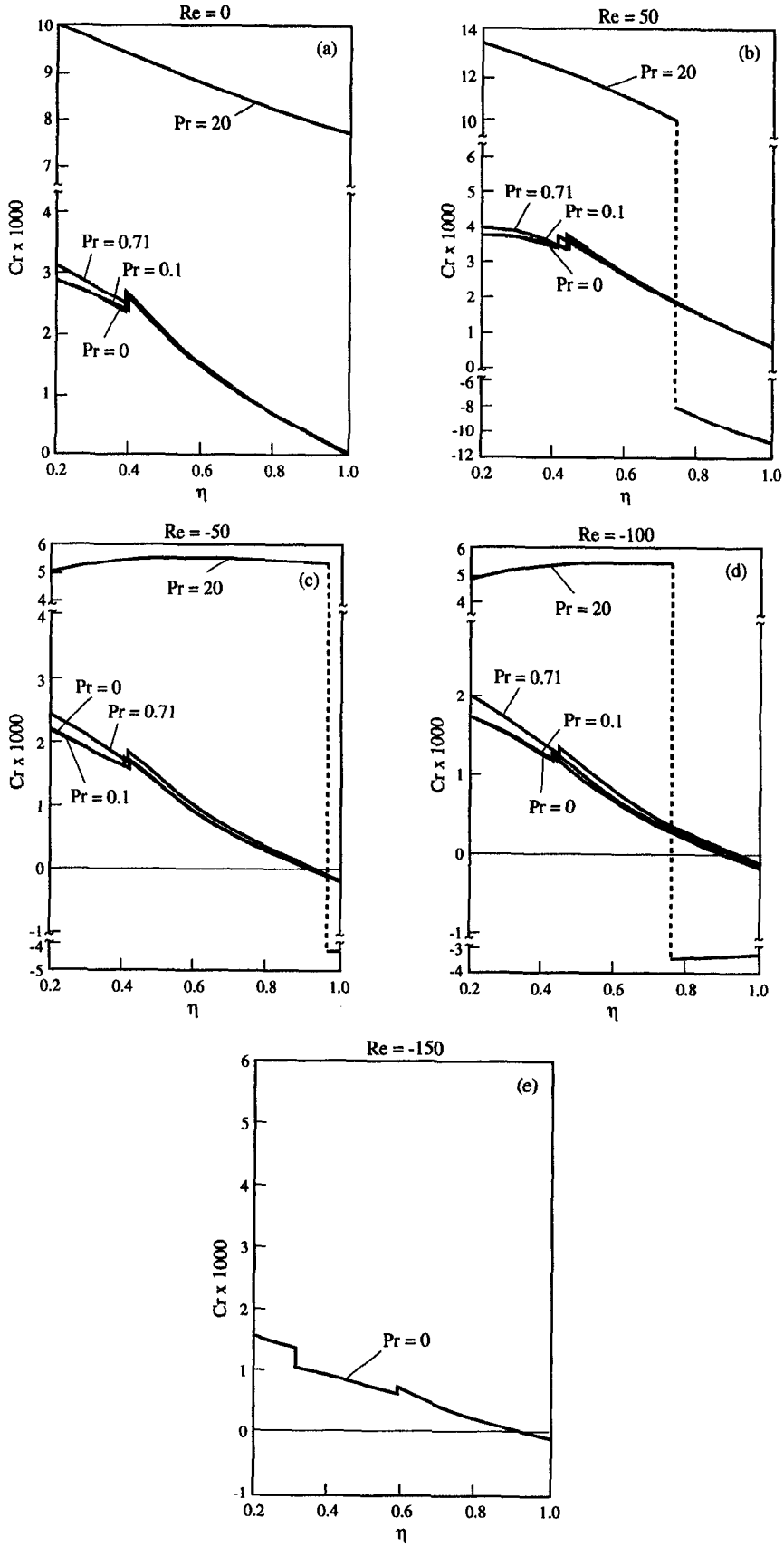

Fig. 5. The critical wave speeds for various values of the Prandtl number as function of the radius ratio: (a) $Re = 0$; (b) $Re = 50$; (c) $Re = -50$; (d) $Re = -100$; (e) $Re = -150$.

decreases except at the transition points. The flow is driven upwards due to the effect of the curvature ($c_r > 0$). For $Re = -50$, -100 and -150, the unstable flow moves downward slightly ($c_r < 0$) due to the downward motion of the inner cylinder as $\eta \to 1$. Therefore, the critical wave speed changes continuously from negative to positive as the curvature increases. For $Re = 50$, the unstable flow is driven upwards. For $Pr = 20$ and $Re \neq 0$, the flow is driven upwards ($c_r > 0$) for smaller radius ratios, while it moves downwards ($c_r < 0$) for larger radius ratios. The critical wave speed for $Re = 0$ and 50 decreases with an increasing radius ratio. The critical wave speed for $Re = -50$ and -100 increases slightly with an increase in radius ratio. The appearance of the point of discontinuity is due to a switch of the buoyant mode, initially induced from the boundary layer near the outer cylinder, and switching to the inner cylinder as the curvature increases.

4. CONCLUSION

The stability of natural convection in a tall vertical annulus with the influence of inner-cylinder motion has been investigated using linear theory. As with the results for the vertical slot [4], when the shear mode is dominant (small Prandtl number fluids), the flow is stabilized by a downward motion of the inner cylinder. It is also destabilized by smaller upward motion and stabilized by faster upward motion. For a small Prandtl number fluid with a smaller radius ratio, the non-axisymmetric disturbance ($m = 1$) is most unstable no matter which direction the inner cylinder is moving. For $Re = -150$, the non-axisymmetric mode ($m = 2$) may replace the mode $m = 0$ and 1 in $0.23 < \eta < 0.58$. When the inner cylinder is moving upwards, the unstable flow is always driving upwards. As the inner cylinder is moving downwards, the unstable flow may change from downward to upward motion as the curvature increases. When the buoyant mode is dominant (high Prandtl number fluids), the flow is stabilized by the motion of the inner cylinder. As the inner cylinder moves, the most unstable mechanism is switched from a buoyant mode generated by the boundary near the outer cylinder to the inner cylinder one with the increase of the curvature.

REFERENCES

1. I. G. Choi and S. A. Korpela, Stability of the conduction regime of natural convection in a tall vertical annulus, *J. Fluid Mech.* **99,** 725–738 (1980).
2. G. B. McFadden, S. R. Coriell and R. F. Boisvert, Asymmetric instabilities in buoyancy-driven flow in a tall vertical annulus, *Physics Fluids* **27,** 1359–1361 (1984).
3. A. A. Mohamad and R. Viskanta, Stability of lid-driven shallow cavity heated from below, *Int. J. Heat Mass Transfer* **32,** 2155–2166 (1989).
4. J.-C. Chen and C.-K. Hsieh, Linear stability of natural convection in a tall vertical slot with a moving side wall, *Int. J. Heat Mass Transfer* **36,** 1471–1476 (1993).
5. J. E. Hart, Stability of the flow in a differentially heated inclined box, *J. Fluid Mech* **47,** 547–576 (1971).

APPENDIX

Equations (4a) and (4b) are derived as follows. Superimposing on equations (2a)–(2f), the equations for an isothermal forced flow, w_1, yields

$$-Gr\frac{dp}{dz} + \frac{1}{r}\frac{d}{dr}\left(r\frac{dw_1}{dr}\right) = 0 \tag{A1a}$$

$$w_1\left(\frac{\eta}{1-\eta}\right) = \frac{Re}{Gr} \tag{A1b}$$

$$w_1\left(\frac{1}{1-\eta}\right) = 0 \tag{A1c}$$

$$\int_{\eta/(1-\eta)}^{1/(1-\eta)} w_1 r\,dr = 0 \tag{A1d}$$

and the equations for a buoyancy-driven flow, w_2, are derived from

$$\frac{1}{r}\frac{d}{dr}\left(r\frac{dw_2}{dr}\right) + (T - T_0) = 0 \tag{A2a}$$

$$w_2\left(\frac{\eta}{1-\eta}\right) = 0 \tag{A2b}$$

$$w_2\left(\frac{1}{1-\eta}\right) = 0 \tag{A2c}$$

$$\int_{\eta/(1-\eta)}^{1/(1-\eta)} w_2 r\,dr = 0. \tag{A2d}$$

The solution of w_1 yields equation (4a):

$$w_1(r) = Ar^2 + B\ln r + C$$

where

$$A = \frac{-Re(1-\eta)(1-\eta^2+2\eta^2\ln\eta)}{Gr(1+\eta)(1-\eta^2+\ln\eta+\eta^2\ln\eta)}$$

$$B = \frac{Re}{Gr\ln\eta} + \frac{A(1+\eta)}{(1-\eta)\ln\eta}$$

$$C = \frac{Re\ln(1-\eta)}{Gr\ln\eta} + \frac{A(1+\eta)\ln(1-\eta)}{(1-\eta)\ln\eta} - \frac{A}{(1-\eta)^2}$$

and the solution of w_2 yields equation (4b)

$$w_2(r) = -\frac{r^2}{4\ln\eta}\ln[(1-\eta)r] + \frac{r^2}{4\ln\eta}\frac{T_0 r^2}{4} + D\ln r + E$$

where

$$T_0 = \frac{(\eta^2 - 1 - \frac{3}{4}\ln\eta - \frac{7}{4}\eta^2\ln\eta)(1-\eta)^2 - \eta^4(\ln\eta)^2}{(1-\eta^2)\ln\eta(\eta^2\ln\eta + \ln\eta - \eta^2 + 1)}$$

$$D = \frac{T_0}{4\ln\eta} + \frac{1}{4(\ln\eta)^2} + \frac{\eta^2}{4(1-\eta)^2\ln\eta}$$

$$E = \frac{(1+\eta)\ln(1-\eta)}{4(1-\eta)(\ln\eta)^2} + \frac{T_0(1+\eta)\ln(1-\eta)}{4(1-\eta)\ln\eta} + \frac{\eta^2\ln(1-\eta)-1}{4(1-\eta)^2\ln\eta} - \frac{T_0}{4(1-\eta)^2}.$$